AIP Advances

Natural discharge after pulse and cooperative electrodes to enhance droplet velocity in digital microfluidics

Tianlan Chen, Cheng Dong, Jie Gao, Yanwei Jia, Pui-In Mak, Mang-I Vai, and Rui P. Martins

Citation: AIP Advances **4**, 047129 (2014); doi: 10.1063/1.4873407
View online: http://dx.doi.org/10.1063/1.4873407
View Table of Contents: http://scitation.aip.org/content/aip/journal/adva/4/4?ver=pdfcov
Published by the AIP Publishing

Natural discharge after pulse and cooperative electrodes to enhance droplet velocity in digital microfluidics

Tianlan Chen,[a] Cheng Dong,[a] Jie Gao, Yanwei Jia, Pui-In Mak,[b] Mang-I Vai, and Rui P. Martins[c]
State Key Laboratory of Analog and Mixed-Signal VLSI and FST-ECE, University of Macau, Macao, China

(Received 27 January 2014; accepted 14 April 2014; published online 23 April 2014)

Digital Microfluidics (DMF) is a promising technology for biological/chemical micro-reactions due to its distinct droplet manageability via electronic automation, but the limited velocity of droplet transportation has hindered DMF from utilization in high throughput applications. In this paper, by adaptively fitting the actuation voltages to the dynamic motions of droplet movement under real-time feedback monitoring, two control-engaged electrode-driving techniques: *Natural Discharge after Pulse (NDAP)* and *Cooperative Electrodes (CE)* are proposed. They together lead to, for the first time, enhanced droplet velocity with lower root mean square voltage value. [http://dx.doi.org/10.1063/1.4873407]

Digital microfluidics (DMF) is a control-engaged droplet-reaction platform that allows complex and scheduling automation on an array of microelectrodes,[1,2] rendering itself a kind of micro total analysis system (μTAS) feasible for a wide variety of chemical and biological applications such as immunoassays,[3] DNA sample processing[4] and cell-based assays.[5] Unlike the traditional fixed-channel microfluidics, DMF is an electronic-centric open platform amenable to different operation protocols by software, streamlining the hardware assembly (e.g., no micropumps and disarray tubes). Conversely, DMF under the principle of electrowetting-on-dielectric (EWOD) is intrinsically inferior in terms of throughput, owing to its inflexible tradeoff between droplet velocity (v_{droplet}) and chip reliability. This v_{droplet} limitation has restricted the DMF technology to enter the high-throughput practices such as cell sorting[6] and drug screening.[7]

To broaden the applications of DMF, recent works have investigated different ways to enhance v_{droplet} by incorporating co-planar electrodes,[8] or conforming water-oil core-shell structure.[9] Yet, both are vulnerable to contamination and evaporation that are intolerable for applications like polymerase chain reaction (PCR).[10] Alternatively, boosting the actuation voltage (i.e., the applied electric field) can also raise v_{droplet}, but compromising the chip lifetime due to the risk of dielectric breakdown,[11] and raising the cost of electronic components which have to withstand higher operating voltages. To our knowledge, there is no electrode-driving technique that can enhance v_{droplet} beyond that with DC actuation signal, while not shortening the electrode lifetime.

As reported,[12] dynamic phases were observed during droplet transportation. The droplet deforms at the initial stage of the actuation on a quasi-equilibrium status, and then reaches to equilibrium status in an oval shape. This quasi-equilibrium status should cause energy loss and lower droplet transporting efficiency. Murren *et al*. have introduced the DC-pulse train[13] actuation signal to avoid droplet deformation, resulting in better v_{droplet} regulation. However, due to the lowered effective

[a]Equal Contribution
[b]E-mail: pimak@umac.mo
[c]on leave from Instituto Superior Técnico, Universidade de Lisboa, Portugal, Portugal

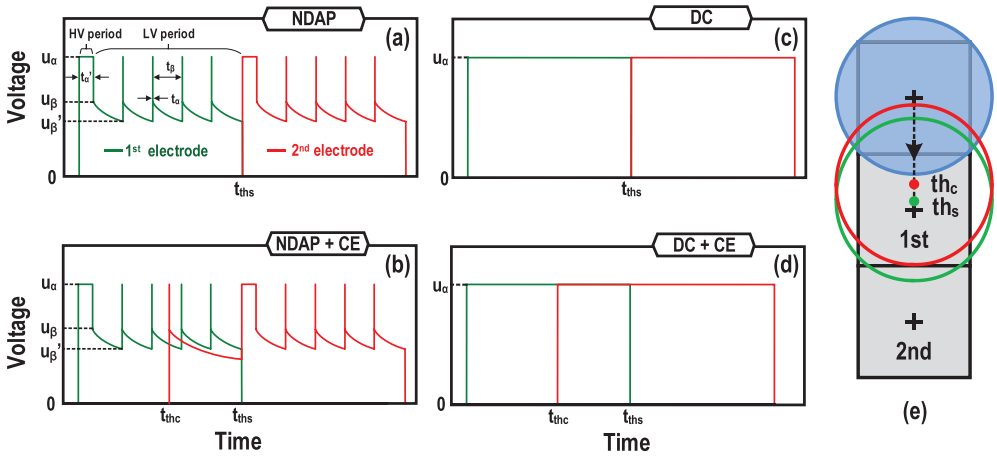

FIG. 1. Sketches of four possible electrode-driving schemes for droplet movements over two electrodes: (a) Natural Discharge after Pulse (NDAP): The high-voltage (HV) period lasts shorter, while the low-voltage (LV) under natural discharge lasts longer with short pulse recharging periodically. (b) DC signal. (c) NDAP with cooperative electrodes (CE) overlaps the charging time of neighboring electrodes. (d) DC plus CE driving. (e) Droplet moving toward two target electrodes and location of the two thresholds on the first target electrode. The electrode was grounded when the charging was done in all schemes.

voltage (i.e., electrodes are energized only alternately), the resultant v_{droplet} still did not exceed that with DC actuation signal.

In this paper, we propose two control-engaged electrode-driving techniques named *Natural Discharge after Pulse (NDAP)* and *Cooperative Electrodes (CE)*, to match the dynamic motions of droplet movement. They together lead to an enhanced v_{droplet} superior to that actuated by DC, while maintaining a lower root mean square (RMS) voltage.

NDAP, as shown in Fig. 1(a), is based on a series of *managed* DC pulses and multi-cycle natural discharging coherent with the droplet dynamics under EWOD. Particularly, we tailor high-voltage (HV) periods, t'_α to kick off the droplet movement and sustain v_{droplet}, and low-voltage (LV) periods, t_β under natural (i.e., exponentially decay under the time constant of resistor-capacitor) discharge to overcome the resistance force for v_{droplet} regulation. Also, the LV period ensures there is sufficient charge to facilitate the tracking of electrode's capacitance for precise real-time droplet positioning. The number of DC pulses, t_α is adaptively calculated according to the dynamic droplet position in real time. As a result, droplets with different hydrodynamics, and electrodes with small imperfection, can still be handled without calibration.

CE is inspired by the fact that when a droplet is transported over a sequence of electrodes, the droplet suffers from deformation and local vibration, lowering the average v_{droplet}, between the gap of the electrodes. In fact, the next target electrode can be *early-charged* before discharging the current one to regulate v_{droplet} over a sequence of electrodes transportation. Guided by the real-time droplet position feedback, the electrodes overlap charging time can be optimally calculated by the software engine, with no extra cost. Also, CE is independent of the actuation waveform. Figs. 1(a) and 1(b) illustrate the cases of NDAP and NDAP + CE, whereas Figs. 1(c) and 1(d) depict the cases of simple DC and DC + CE, respectively. Two crucial timing t_{ths} and t_{thc} are defined as: the leading edge of the droplet to reach the next electrode, and the droplet's center to overlap with that of the target electrode, respectively. For NDAP + CE, the charging is specialized to pulse the second electrode after t_{ths}. For DC + CE, the charging of the two adjacent electrodes was overlapped. CE should be started right on time, requiring a feedback to track the droplet position in real time and perform self-optimization. The CE is triggered when the monitored position reaches the predefined thresholds th_s and th_c as shown in Fig. 1(e).

In order to integrate NDAP and CE into the actuation signal, a real-time precise droplet positioning feedback control[14] is required. In our experiments, an electronic control system programmed by software is developed to realize the desired dynamic actuation waveform. The prototype DMF system consists of three subsystems (Fig. 2): (*i*) the control electronics (discrete components on

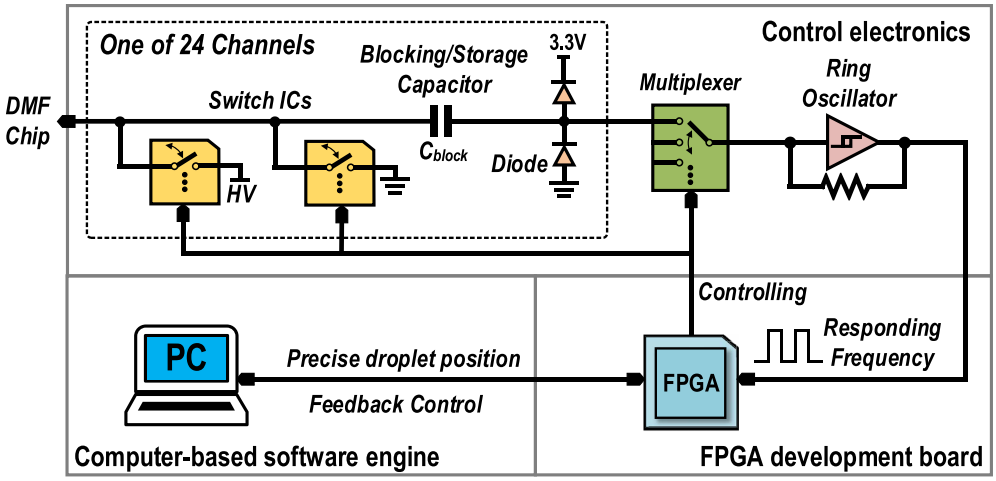

FIG. 2. Real-time position feedback control system. Actuation high voltage signal to the electrodes is controlled by the switch ICs (CPC7220) and blocked by blocking capacitor to the ring oscillator. Real-time feedback of droplet position is acquired by the FPGA via the responding frequency of a ring oscillator. A computer-based software engine controls the switch ICs through the FPGA according to the feedback data.

printed circuit board, PCB), (*ii*) the field programmable gate array (FPGA), and (*iii*) the computer-based software engine. First, FPGA collects the capacitance-derived frequency data and sends it to the computer. Second, the computer software calculates the precise droplet position and generates the durations of the actuation signal. Finally, the control electronics implements NDAP/CE under the guide of the FPGA.

Note that the voltage amplitude of NDAP varies by managed pulses, similar to low-frequency AC signal, which has been reported to reduce the contact-line friction and therefore enhance the droplet velocity.[15] NDAP is a unipolar actuation signal based on DC which would be highly desirable for analysis of some charged biological samples as DNA for solving the sticking problem.[16] The real-time droplet positioning feed-back system associated with NDAP also offers big flexibility to fit the pulsing actuation signal to the droplet dynamics, which is absent in AC actuation system.

The DMF devices were fabricated and assembled following the protocols described previously.[14] Here, a drop of aqueous solution (~0.5 μL) immersed in silicon oil (1 cSt) (Sigma-Aldrich, MO) was sandwiched by a bottom glass and a top Indium Tin Oxide (ITO, Kaivo Optoelectronic) glass with a 0.25 mm spacer. Chromium electrodes (1 mm × 1 mm) are separated from each other with a 0.01 mm gap patterned on the bottom glass. A dielectric layer of Ta_2O_5 (250 nm) was coated on the electrodes followed by a layer of Parylene C (480 nm) (Galxyl) and then a hydrophobic layer of Teflon AF 1600 (100 nm) (DuPont). The top ITO glass (Kaivo, ITO-P001) was coated with a hydrophobic layer of 100 nm Teflon. In the experiments design and data analysis, Analysis of Variance (ANOVA) was used to evaluate the significance of data.

NDAP is an irregular voltage signal as shown in Fig. 1(a). Its RMS voltage can be determined by,

$$V_{RMS,total} = \sqrt{\frac{t_1}{t_{total}} {V_{RMS,1}}^2 + \frac{t_2}{t_{total}} {V_{RMS,2}}^2 + \ldots + \frac{t_n}{t_{total}} {V_{RMS,n}}^2} \quad (1)$$

where the contribution of each period of the signal is weighted by time. As a special case, the RMS voltage of a DC signal, u_α, equals to the peak voltage. During the natural discharge period, the corresponding voltage of the residual charge is given by,

$$u_{res} = u_\beta e^{-t/\tau} \quad (2)$$

where u_{res} is the voltage applied to the electrode, u_β is the discharge period initial voltage, t is the elapsed time, and τ is the RC (Resistance-Capacitance) time constant, which is defined as

TABLE I. RMS voltages of NDAP.

HV level time (ms)	LV level time (ms)	RMS value (V)
1	299	10.74
3	297	10.77
5	295	10.81
7	293	10.84
9	291	10.87
11	289	10.92
13	287	10.94
50	250	11.53
100	200	12.30
150	150	13.10
200	100	13.69
250	50	14.34
300[a]	0	15.00

[a]It is equivalent to DC signal.

$\tau = R_{equivalence} \times C_{block}$. Then, the RMS value among this period is given by,

$$V_{RMS,discharge} = \sqrt{\frac{1}{t_\beta}\int_0^{t_\beta} {u_{res}}^2 dt} \tag{3}$$

where $V_{RMS,discharge}$ is the RMS value over t_β. Substituting the (2) into (3) yields,

$$V_{RMS,discharge} = u_\beta \sqrt{\frac{\tau}{2t_\beta}(1 - e^{-2t_\beta/\tau})} \tag{4}$$

Thus, the actual RMS value in a droplet movement actuation by NDAP is given by,

$$V_{RMS,total} = \sqrt{\frac{t'_\alpha + (n-1)\,t_\alpha}{t'_\alpha + (n-1)\,nt_\alpha + nt_\beta}{u_\alpha}^2 + \frac{n\tau}{2(t_\alpha{}' + (n-1)t_\alpha + nt_\beta)}(1 - e^{-2t_\beta/\tau}){u_\beta}^2} \tag{5}$$

The equivalent resistance $R_{equivalence}$ between the individual electrode and ground was measured as ~5 MΩ on an average of totally 24 electrodes, and C_{block} was measured as ~450 nF, giving a time constant value, τ, of 2.25. When u_α was set at 15 V, u_β and u'_β were 11.1 and 10.1 V, respectively, under t_β = 90 ms. Table I shows the RMS voltage in NDAP system with different values of HV period, t'_α. Obviously, the RMS voltage of NDAP was up to 4 V smaller than DC. We have verified the accuracy of the calculation by comparing the calculated RMS voltage with that measured by an oscilloscope, yielding less than 2% deviation.

To assess the performance of NDAP, we compared v_{droplet} of DI water driven by NDAP with that driven by DC which is highly desirable to use in on-chip DNA analysis given that a negative charge inhibits the DNA adhesion on chip surface.[16] Different value of t'_α of NDAP was tested and compared with DC in Fig. 3(a), while NDAP and DC shared the same peak voltage value, u_α = 15 V. To eliminate the variation among batches of experiments due to slight changes in the volume of a droplet, all the velocities were normalized to the average velocity under DC actuation. NDAP showed a low efficiency of droplet transportation while t'_α was smaller than 13 ms. When the value of t'_α was between 13 and 100 ms, the average v_{droplet} of NDAP was larger than DC. A further increase of t'_α bigger than 100 ms did not add more values, and the velocity returned back to that of DC. ANOVA proved that the data were statistically significant ($p < 0.01$).This phenomenon can be related to the droplet dynamics during the transportation.[12] For a very short first pulse, the driving force would be inadequate to move the droplet to an optimum velocity, though the residual charge in the electrode may still pull the droplet forward in the LV period. In fact, if the first pulse in NDAP was sufficient to make the droplet enter the equilibrium state, the whole droplet would start to move in a stretching conformation. The retreat of the force would cause the droplet to relax and

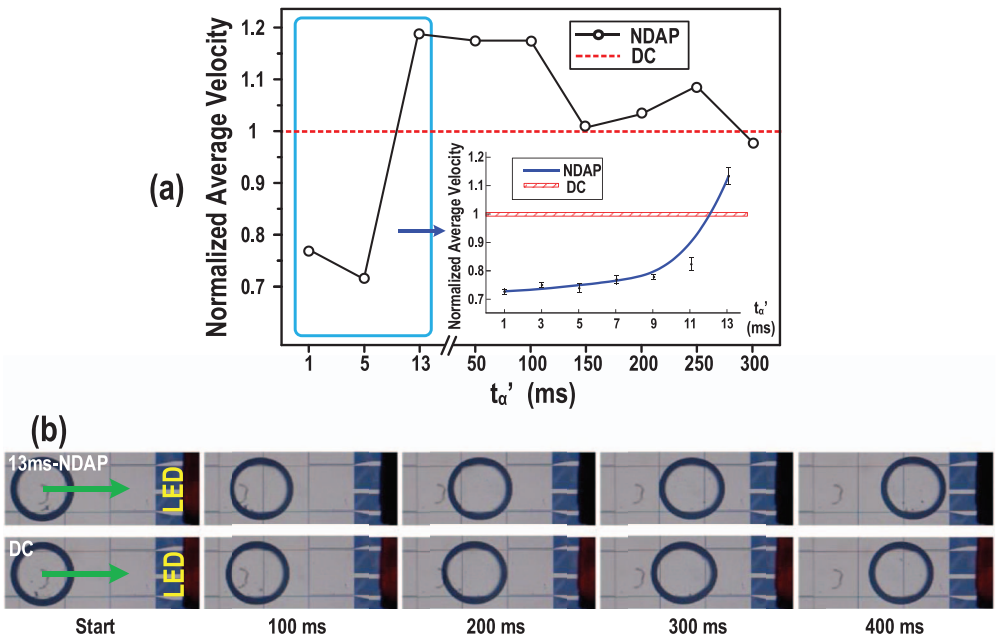

FIG. 3. (a) Normalized average velocity of a droplet under NDAP signals with different t'_α and DC. Inserted curve shows the droplet velocities with $t'_\alpha < 13$ ms. The data were normalized at the average velocity under DC. (b) Video frames of a droplet actuated by NDAP and DC crossing 2 electrodes (Multimedia view) [URL: http://dx.doi.org/10.1063/1.4873407.1] . Video was captured by a high speed camera (Nikon V2), which has a maximum frame rate up to 1200 frames/second (resolution 320 × 120 pixels). A LED light was set in the same frame to light on when the electrode was being charged. Individual frames extracted from the videos were analyzed by the image processing software *Image J* to obtain the $v_{droplet}$.

back to a round shape (i.e., equilibrium status) as much as possible. This status would maximize the driving-force efficiency, which as a consequence would enhance the droplet transportation by NDAP even faster than DC due to its high-driving efficiency. Fig. 3(b) (Multimedia view) shows the captures from the video which clearly indicated that 13ms-NDAP signal had a higher electrode driving efficiency.

Conventionally, when a droplet is transported over a row of electrodes, only one individual electrode is charged. It had been observed that $v_{droplet}$ decelerated significantly when the center of a droplet approached that of the electrode, being a main factor limiting the average $v_{droplet}$. When we cooperatively charged two adjacent electrodes (CE), the deceleration phenomenon was greatly inhibited. Fig. 4 shows the velocity of NDAP (13 ms, t'_α) and DC enhanced by CE. Obviously, at ~0.95 mm, the minimum $v_{droplet}$ under CE was higher than that without enhancement. The same improvement can be seen on the DC case as well.

As shown above NDAP + CE had dramatically improved the transportation characteristics of a droplet between two adjacent electrodes compared with that driven by DC. A droplet moving across 12 electrodes arranged by a 2 × 6 matrix driven by either NDAP + CE or DC only was monitored and studied. The traces of the centroids of the moving droplet are shown in Fig. 5(a) (Multimedia view) and 5(b) (Multimedia view). It shows that when more electrodes were involved with the same running conditions, the enhancement was indeed more obvious. The DC signal charging time was fixed empirically at 260 ms (just adequate to transport the droplet to the next electrode) and t'_α of NDAP was 13 ms. The whole running time was set at 3 s such that the droplet driven by NDAP + CE could complete a whole travel and return to the origin. However, during the same charging period, the droplet driven by DC only completed 10 electrodes. The average time for the droplet to move across single electrode for NDAP + CE and DC signals were 223 and 260 ms, with average velocities of 4.48 and 3.84 mm/s, respectively.

The detailed velocity analysis is shown in Fig. 5(c). It can be seen that NDAP + CE dramatically and reliably reduced the decrease of velocity between two adjacent electrodes. The velocity of NDAP

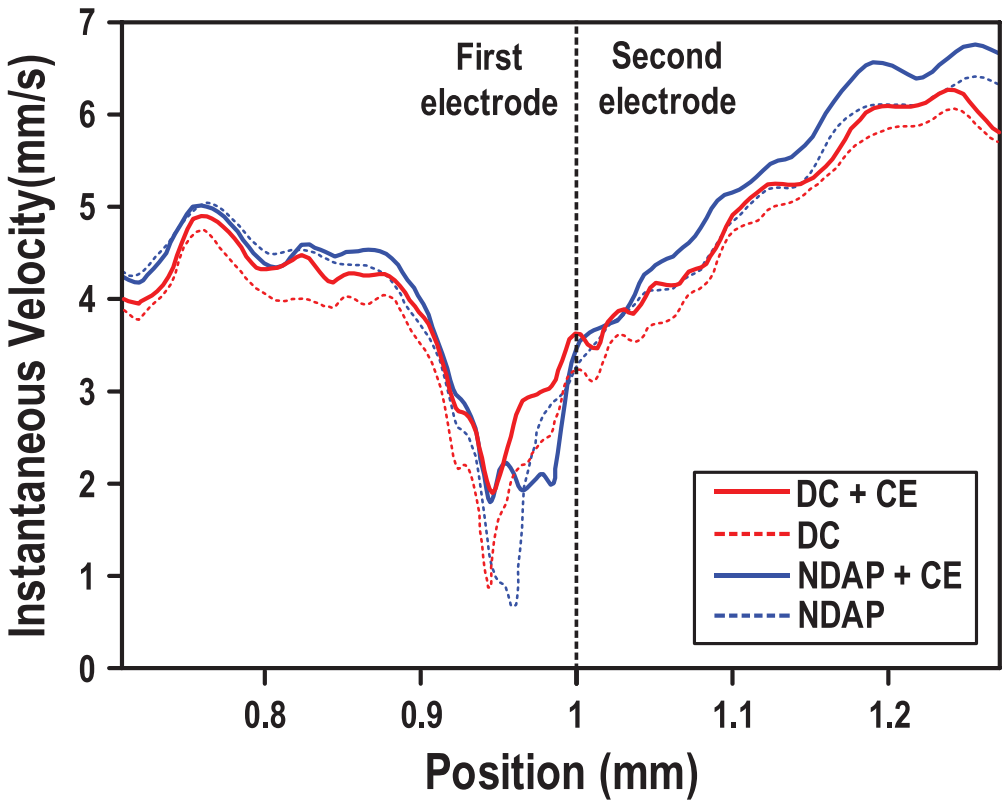

FIG. 4. Comparison between individual and cooperative electrode-driving techniques in terms of transportation velocity. Each shown curve was an average of 10 curves under same conditions ($p < 0.01$).

+ CE at electrode No. 6 was smaller than that of DC. Moreover, the total time of getting through the corner (No. 6, 7 and 8) was much shorter (620 ms) than that of DC (780 ms). The direction change toward electrode No. 7 of NDAP + CE was also earlier than DC. This curved movement could be very useful in terms of quickly mixing/circulating of droplets on chip.

As shown in Figure 5(c), when a droplet moves along an electrode, the velocity is not constant. It vibrates across each electrode. We analyzed the velocities in groups as maximum, minimum and in average to find out which part NDAP + CE significantly enhanced to improve its overall transportation efficiency. Figure 5(d) shows that the minimum velocities were greatly enhanced by 2.5 times by NDAP + CE while the maximum velocities are comparable between NDAP + CE and DC. This causes an overall increase in the average velocity of 16.6% by NDAP + CE. The significance of the data had been tested ($p < 0.01$).

Raising the DC voltage could greatly improve the droplet transportation velocity.[9] As a DC based manageable pulse actuation, NDAP can be used at any voltage. In another word, no matter what DC voltage is used to improve the droplet transportation, switching to NDAP + CE would gain another 15% over the enhancement. Especially for a high DC voltage, NDAP + CE would be more preferred for its low RMS value has less possibility in shortening the lifetime of the electrode due to dielectric breakdown.[17]

In summary, we have introduced two electrode-driving techniques, Natural Discharge after Pulse (NDAP) and Cooperative Electrodes (CE), with a real time feedback control in DMF and speeded up the droplet movement beyond those achieved by conventional actuation signal via matching the droplet dynamics with the strength and duration of the applied electric field. The entire scheme involves only low-cost electronics and software programming. That gives the feasibility to be upgraded for further researches, customized to other applications, and easily repeated by others.

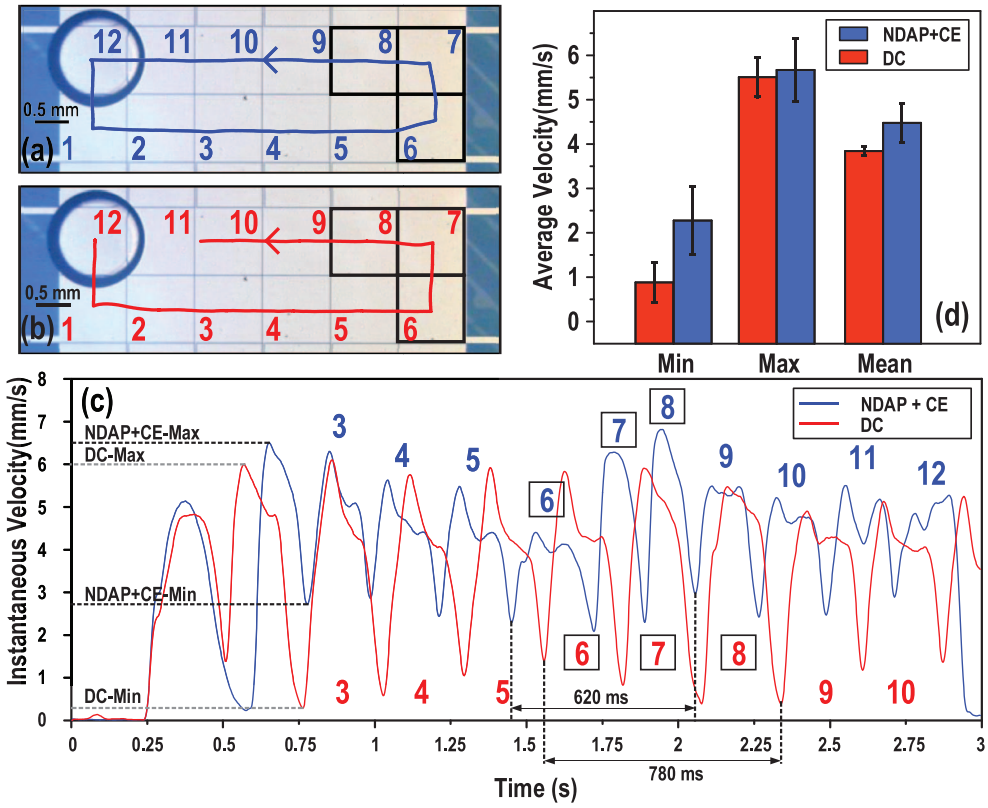

FIG. 5. Comparison between the proposed (NDAP + CE and high-speed feedback) and classical (DC) schemes for droplet movements in a long run of 3 s: (a) Droplet successfully moved across 12 electrodes when it was controlled by NDAP + CE. The path of the droplet's center had been shortened at electrode No. 6 by CE, which charged electrode No. 7 before the droplet reached electrode No. 6, resulting in an upward move of droplet in advance. The whole droplet transportation was recorded in video (Multimedia view) [URL: http://dx.doi.org/10.1063/1.4873407.2] . (b) Droplet failed to complete movement in 3 s due to its lower speed. The moving path was close to the right angle at the two corners. The whole droplet transportation was recorded in video (Multimedia view) [URL: http://dx.doi.org/10.1063/1.4873407.3] . (c) Instantaneous velocity of the droplet moving across the electrodes. As expected, droplet controlled by the proposed scheme moved across electrode No. 6-7-8 using a much shorter time than that of the classical procedure. (d) Average velocities of minimum/maximum instantaneous velocities and mean velocities across each electrode.

ACKNOWLEDGMENTS

This work was supported by the Research Committee of University of Macau and Macao Science and Technology Development Fund (FDCT, No. 033/2011/A2).

[1] M. G. Pollack, R. B. Fair, and A. D. Shenderov, Applied Physics Letters **77**(11), 1725 (2000).
[2] M. G. Pollack, A. D. Shenderov, and R. B. Fair, Lab on a Chip **2**(2), 96 (2002).
[3] M. J. Schertzer, R. Ben Mrad, and P. E. Sullivan, Sens. Actuator B-Chem. **164**(1), 1 (2012).
[4] R. Sista, Z. S. Hua, P. Thwar, A. Sudarsan, V. Srinivasan, A. Eckhardt, M. Pollack, and V. Pamula, Lab on a Chip **8**(12), 2091 (2008).
[5] S. Srigunapalan, I. A. Eydelnant, C. A. Simmons, and A. R. Wheeler, Lab on a Chip **12**(2), 369 (2012).
[6] E. M. Miller, A. H. C. Ng, U. Uddayasankar, and A. R. Wheeler, Anal. Bioanal. Chem. **399**(1), 337 (2011).
[7] T. Thorsen, S. J. Maerkl, and S. R. Quake, Science **298**(5593), 580 (2002).
[8] A. N. Banerjee, S. Z. Qian, and S. W. Joo, J. Colloid Interface Sci. **362**(2), 567 (2011).
[9] D. Brassard, L. Malic, F. Normandin, M. Tabrizian, and T. Veres, Lab on a Chip **8**(8), 1342 (2008).
[10] Y. W. Jia, P. I. Mak, C. Massey, R. P. Martins, and L. J. Wangh, Lab on a Chip **13**, 4635 (2013).
[11] W. C. Nelson and C. J. Kim, J. Adhes. Sci. Technol. **26**(12–17), 1747 (2012).
[12] R. Baviere, J. Boutet, and Y. Fouillet, Microfluidics and Nanofluidics **4**(4), 287 (2008).
[13] M. A. Murran and H. Najjaran, Applied Physics Letters **101**(14), 144102 (2012).

[14] J. Gao, X. M. Liu, T. L. Chen, P. I. Mak, Y. G. Du, M. I. Vai, B. C. Lin, and R. P. Martins, Lab on a Chip **13**(3), 443 (2013).
[15] N. Kumari, V. Bahadur, and S. V. Garimella, Journal of Micromechanics and Microengineering **18**(10), 105015 (2008).
[16] M. Erdmann, R. David, A. Fornof, and H. E. Gaub, Nat. Nanotechnol. **5**(2), 154 (2010).
[17] S. K. Cho, H. J. Moon, and C. J. Kim, J. Microelectromech. Syst. **12**(1), 70 (2003).